J Pathol Inform

Editor-in-Chief:
Anil V. Parwani , Pittsburgh, PA, USA
Liron Pantanowitz, Pittsburgh, PA, USA

OPEN ACCESS
HTML format

For entire Editorial Board visit : www.jpathinformatics.org/editorialboard.asp

Research Article

A nuclear circularity-based classifier for diagnostic distinction of desmoplastic from spindle cell melanoma in digitized histological images

Manuel Schöchlin[1], Stephanie E. Weissinger[1], Arnd R. Brandes[2], Markus Herrmann[1,3], Peter Möller,[1] Jochen K. Lennerz[1]

[1]Institute of Pathology, University Ulm, [2]Institut für Lasertechnologien in der Medizin und Meßtechnik, University Ulm, Ulm, Germany, [3]Institute of Molecular Life Sciences, University of Zurich, Zurich, Switzerland

E-mail: *Jochen K. Lennerz - jochen.lennerz@uni-ulm.de
*Corresponding author

Received: 16 June 14 Accepted: 06 Sep 14 Published: 21 October 2014

This article may be cited as:
Schöchlin M, Weissinger SE, Brandes AR, Herrmann M, Möller P, Lennerz JK. A nuclear circularity-based classifier for diagnostic distinction of desmoplastic from spindle cell melanoma in digitized histological images. J Pathol Inform 2014;5:40.

Available FREE in open access from: http://www.jpathinformatics.org/text.asp?2014/5/1/40/143335

Abstract

Context: Distinction of spindle cell melanoma (SM) and desmoplastic melanoma (DM) is clinically important due to differences in metastatic rate and prognosis; however, histological distinction is not always straightforward. During a routine review of cases, we noted differences in nuclear circularity between SM and DM. **Aim:** The primary aim in our study was to determine whether these differences in nuclear circularity, when assessed using a basic ImageJ-based threshold extraction, can serve as a diagnostic classifier to distinguish DM from SM. **Settings and Design:** Our retrospective analysis of an established patient cohort (SM n = 9, DM n = 9) was employed to determine discriminatory power. **Subjects and Methods:** Regions of interest (total n = 108; 6 images per case) were selected from scanned H and E-stained histological sections, and nuclear circularity was extracted and quantified by computational image analysis using open source tools (plugins for ImageJ). **Statistical Analysis:** Using analysis of variance, t-tests, and Fisher's exact tests, we compared extracted quantitative shape measures; statistical significance was defined as $P < 0.05$. **Results:** Classifying circularity values into four shape categories (spindled, elongated, oval, round) demonstrated significant differences in the spindled and round categories. Paradoxically, DM contained more spindled nuclei than SM ($P = 0.011$) and SM contained more round nuclei than DM ($P = 0.026$). Performance assessment using a combined shape-classification of the round and spindled fractions showed 88.9% accuracy and a Youden index of 0.77. **Conclusions:** Spindle cell melanoma and DM differ significantly in their nuclear morphology with respect to fractions of round and spindled nuclei. Our study demonstrates that quantifying nuclear circularity can be used as an adjunct diagnostic tool for distinction of DM and SM.

Key words: Digital pathology, morphometry, numerical histology

Access this article online

Website: www.jpathinformatics.org

DOI: 10.4103/2153-3539.143335

Quick Response Code:

INTRODUCTION

Cellular shape, as an integral part of the cellular theory, remains the primary means for groundbreaking recent discoveries.[1,2] In pathology, rendering a diagnosis rests in large parts on the skill of pattern and shape-recognition

for appropriate classification,[3] and for the foreseeable future, microscopy will remain a cornerstone of surgical pathology.[4] Simultaneously, the digital revolution and specifically the adaptation of imaging methods into diagnostics,[5] continues to accelerate progress,[6-11] including advanced imaging methods[12] and computerized quantitative algorithms.[3] Computer-assisted quantitative histology is already applied as an adjunct diagnostic tool in some cases. For example, digital quantification of stained-elements (e.g. human epidermal growth factor receptor 2-immunolabeling intensity) has become part of the repertoire for many diagnostic pathologists.[11,13-15] Despite various studies reporting on classification of morphometric[3] and in particular nuclear features,[16-21] these shape-based quantification tools are not widely established in routine surgical pathology. In contrast, there are several recent basic-science examples of clever combinations of computational morphometry, molecular-genetic, and functional methods.[1,20,22-25] The lack of adoption in the routine diagnostic setting is particularly surprising given that morphometry can provide clinically relevant information[8,17,20,26] and is able to solve diagnostic problems.[16-21,26,27] Due to the drastically increasing performance and adoption of imaging solutions in pathology, one key opportunity of digital pathology quantitative shape-assessment, is largely unexplored.

During routine histological review of several melanoma subtypes, we noted nuclear shape variations between two diagnostic subgroups. Briefly, the two examined melanoma subtypes were spindle cell melanoma (SM) and desmoplastic melanoma (DM). While the one (SM) can essentially occur anywhere in the body and typically presents with widespread metastatic disease, the other (DM) typically occurs in the head-and neck region and has a substantially lower rate of nodal metastasis.[28] Notably, SM and DM are composed of spindle-shaped cells, both are typically amelanotic, and both can be negative for otherwise reliable melanoma immunomarkers. Thus, diagnostic distinction of SM and DM can be challenging. Nuclear-morphometric studies have been conducted in a variety of melanocytic lesions,[16,19,29-31] to our knowledge, however, the spectrum of nuclear shapes in SM and DM has not been studied. Using freely available computational image analysis tools, we carried out a quantitative examination of the nuclear circularity in our SM/DM cohort. The primary aim of our study was to determine whether differences in nuclear circularity can serve as a diagnostic classifier to distinguish SM from DM.

Based on differences in their relative composition of nuclei with distinct nuclear morphologies (i.e. circularity values), we adopted and tested a shape-based classifier to distinguish DM from SM. Examination of the diagnostic performance measures in this particular setting provides proof of principle that quantification of nuclear circularity can be used as an adjunct diagnostic tool in this specific setting.

SUBJECTS AND METHODS

Study Cohort and Tissue Samples

Cases (DM, n = 9; SM, n = 9) were identified by computer-assisted archival searches and excluded when there was no material or slides available for review. We used formalin-fixed, and paraffin-embedded tissues, that was sectioned at 2 μm and H&E stained. At least two board-certified pathologists reviewed each case and confirmed the diagnosis. The applied morphological criteria followed prior publications.[28,32-35] Briefly, SM and DM are composed of an invasive proliferation of spindled/fusiform melanocytes that are separated by desmoplasia composed of dense collagen fibers or fibrous stroma. Based on the degree of desmoplasia the following subtypes can be assigned: DM (≥90%), mixed (≥10-90% desmoplasia) or SM (<10%).[28]

Slide Digitization and Image Capture

Selected H&E-stained sections were scanned using an ×40 objective (final magnification, ×400) on a".slide" scanning system (Olympus; Hamburg, Germany ".slide" version 1. 2) or a Scancope XT Scanner System (Aperio, Vista, CA, USA), as previously described.[36] Each scan was visually inspected for scan-quality before subsequent review and analysis. Digitized slides (file size range: 0.4-7.1GB; total: 51.5 GB) were stored in .vsi (Olympus, Hamburg, Germany) or .svs (Aperio, Vista, CA, USA) file-format. Digital slides were reviewed, and the senior author outlined tumor regions. The first author (M. S.), initially blinded to the primary diagnosis, chose at least 6 representative regions of interest (18 cases × 6 fields = 108 regions of interest). Fields were prioritized when mainly composed of tumor cells with a small nontumor cell component and minimal sectioning-, tissue-, or staining artifacts. Images were captured at a resolution of 0.65 megapixels and stored using the .jpeg file format.

Image Analysis

Processing of each image consisted of a consecutive series of algorithms implemented as plugins in the freely available software ImageJ (http://imagej.nih.gov/ij/; last accessioned August 19, 2014). First, a color deconvolution step achieved segmentation of nuclei as previously described.[37-39] Briefly, the image is deconvoluted into separate color channels and subsequently, the hematoxylin-containing channel (i.e. R-channel of the RGB-color space) is extracted and used for pixel intensity-based threshold segmentation.[36-40] Next, the outlines of segmented nuclei are determined using edge detection algorithms based on differential brightness cut-offs. For the analysis of extracted image

elements, we applied the "analyze particle" filtering and chose the following three measurements for analysis: Circularity (defined as: 4*π*area/perimeter^2), aspect ratio (defined as major_axis/minor_axis) and solidity (defined as area/convex_area) using ImageJ.[41] For circularity, the form factors 1.0 (representing a perfect circle) and 0 (representing a straight line) were excluded from subsequent analyses. We classified nuclei based on factor values, representing the nuclear shapes, into four categories: Spindled (circularity values > 0-0.35), elongated (circularity ≥ 0.35-0.6), oval (circularity ≥ 0.6-0.8), and round (circularity ≥ 0.8-<1.0). A previously reported customized link connected several software platforms (Adobe Photoshop CS3 Adobe Systems, San Jose, CA; Aperio ImageScope; ImageJ version 10.2 or v1.47f).[36]

Data and Statistical Analysis

Measurements were exported for each particle into a database that tracked data regarding the case, image and position for within- and between-tumor comparisons. The measured data did not support the assumption of a Gaussian distribution of shape-based measures. Thus, we chose nonparametric statistical tests. Specifically, we employed the Mann–Whitney test for comparison at the individual measurement level, the Kruskall–Wallis test for comparisons of means at the case-level, and one-way analysis of variance (ANOVA) to compare means in the SM and DM groups (using the posttest Bonferroni correction). For the visualization of case-to-case comparisons (9 SM vs. 9 DM) we generated heatmaps using the "pheatmap" library in the R programming environment (http://www.r-project.org; version 2.13.2). All data were analyzed by using Prism 5.0b (GraphPad Software Inc., La Jolla, CA, USA), Microsoft Excel 2008 (Microsoft Corporation, Redmond, WA, USA), or the online statistical toolkit http://www.hutchon.net/EPRval.htm (last accessioned, November 11, 2013). $P < 0.05$ were regarded as statistically significant.

RESULTS

Our archival searches identified 18 cases of SM/DM that we used as our study cohort. Pertinent features of the study cohort are summarized in Table 1. Briefly, these features are in accord with prior publications[32-35] and we consider our study set representative. Classic examples of the histological appearance are shown in Figure 1a and b. Spindled, amelanotic tumor cells characterize both melanomas. In the case of DM these cells are separated by dense fibrous connective tissue.[28,32-35] During routine microscopic review, we noted differences between the spindled, cytoplasmic outlines and the nuclear shape. Specifically, we noted that in SM, a fraction of tumor cells (with an overall spindled cytoplasmic outline) contain more round nuclei than the spindled cells in DM. Based on this initial observation, we decided to examine the spectrum of nuclear circularity in SM/DM.

Table 1: Clinicopathological characteristics of the study cohort

Characteristic	SM (*n*=9)		DM (*n*=9)		*P* (SM vs. DM)
	Number of cases	Percentage	Number of cases	Percentage	
Age					
Median	65		87		0.04
Range	48-82		53-96		
Sex					
Female	2	22	6	67	0.15
Male	7	78	3	33	
Location					
Head and neck	1	11	8	89	0.003
Trunk	8	89	1	11	
Extremities	0	-	0	-	
Pigmentation					
Yes	4	44	0	0	0.08
No	5	56	9	100	
Stage					
IA	1	11	1	11	0.96
IB	2	22	1	22	
IIA	1	11	2	11	
IIB	3	33	3	33	
III	0	-	0	-	
IV	2	22	2	22	

P values derived from Student's *t*-test (age) Fisher's exact (sex, pigmentation) or Chi-square test (location, stage). SM: Spindle cell melanoma, DM: Desmoplastic melanoma

One of the authors, blinded to the primary diagnosis, captured a total of 108 regions of interest (6 images × 18 cases). These regions were then computationally analyzed using ImagJ software. Given that we applied ImageJ-plugins ("as-is"), the nuclear extraction step carries some limitations, for example, due to prominent nucleoli or nuclear anisochromasia. A representative image illustrating these limitations is depicted in Figure 2a. The image segmentation step for nuclear detection within tissues could be subject to further improvement; however, this missegmentation adds "nonround" features to the SM-group. Since our initial observation and hypothesis was that SM might be characterized by a higher fraction of round nuclei – accepting these imperfections can be regarded as the more pessimistic assumption for hypothesis testing (see Discussion).[42] Readouts for circularity (and for comparison aspect ratio and solidity) were tabulated and a summary of the measurements is provided in Table 2. Simple comparison of mean values between histotypes did not reveal striking differences; however, additional modes of individual case-comparisons suggested substantial variation within and between histotypes [Table 2]. Specifically, when performing analysis of variance of individual cases (ANOVA with posttest correction), we noted significant differences between SM and DM (which was not the case for aspect ratio or solidity; shown for comparison only).

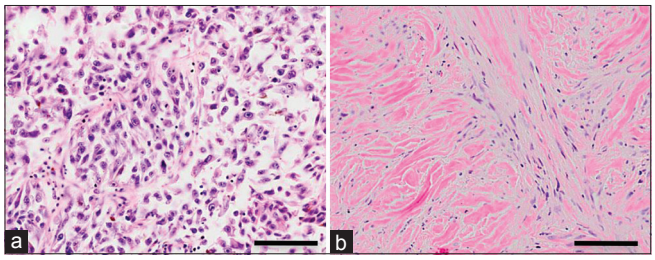

Figure 1: Classic histological appearance of spindle cell melanoma (SM) and desmoplastic melanoma (DM). (a) SM. (b) DM. Both melanomas are typically composed of amelanotic spindled cells. In desmoplastic melanoma thick strands of fibrous/collagenous tissue separate the neoplastic melanocytes. Note: Despite the spindled configuration of cytoplasmic outlines, the nuclear shape (i.e. circularity) differs between SM and DM. Scale bar corresponds to 100 μm

To assess whether variation between entities is represented on an individual case-basis, we performed comparison at the case-level and plotted significant versus nonsignificant *P* values. The results of these comparisons are depicted as 9 × 9 matrix plots [Figure 2b]. When grouping SM and DM together, larger 2 × 2 square-sets (i.e. upper left SM vs. SM and lower right DM vs. DM; separated by black lines) allow visual assessment of the total number of significant differences [red squares in Figure 2b]. Evaluation of the matrix plots showed that circularity demonstrates a large number of statistically

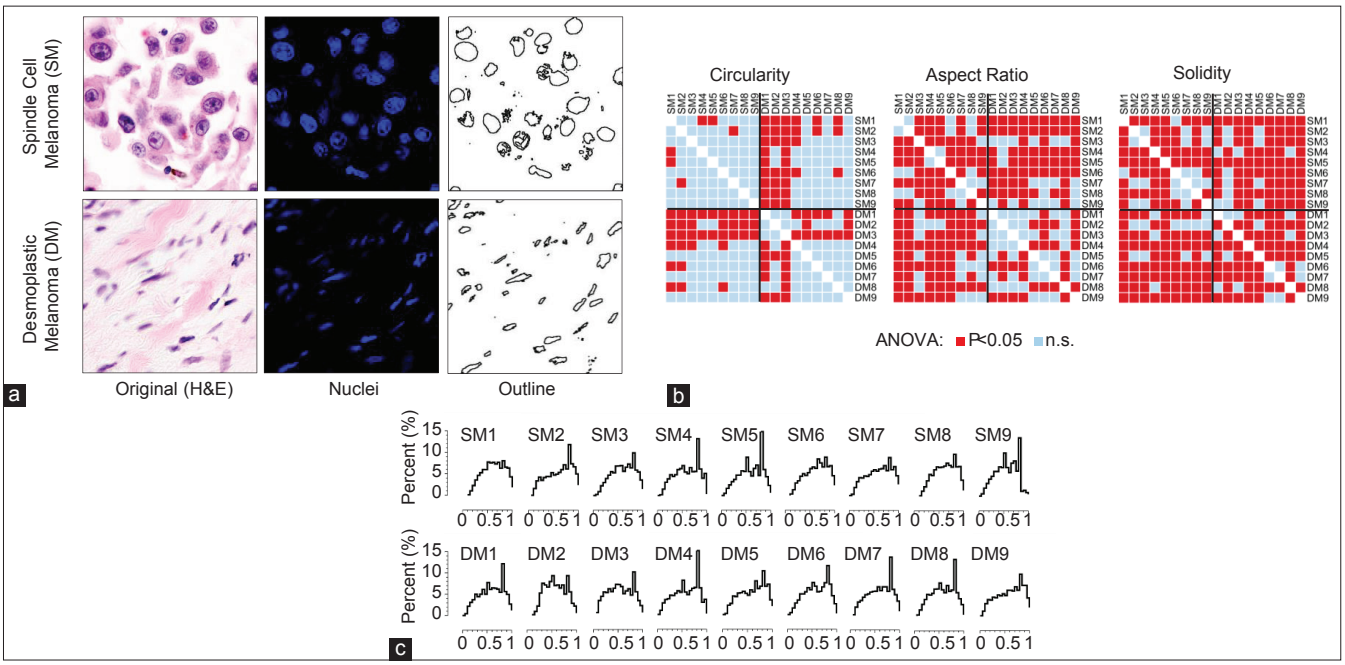

Figure 2: Image processing and feature comparison. (a) Image processing of the original H and E (left) consisted of three steps: Left, spindle cell melanoma (SM) and desmoplastic melanoma (DM) high-power fields were captured; middle, nuclear threshold-based segmentation; and right, edge detection. The resulting image ("outline") served as the source file for subsequent image analysis. Note, that the depicted images also illustrate some of the limitations of the threshold-based nuclear feature extraction (e.g., imposed by nucleoli or nuclear anisochromasia). (b) Results of the case-by-case comparison (9 × 9 correlation matrix plots) using analysis of variance analyses depicted for circularity and for comparison with other shape-measure (i.e., aspect ratio and solidity). (c) Histograms of the frequency distribution for circularity values (total range: 0.024-0.998 with 0 representing a straight line and 1 a perfect circle). Note differences in distribution between SM (top row) versus DM (bottom row)

Table 2: Results of the nuclear circularity classifier

Case	Mean±SD		
	Circularity	Aspect ratio	Solidity
SM			
SM 1	0.608±0.215	1.94±0.730	0.800±0.098
SM 2	0.596±0.246	1.96±0.732	0.771±0.106
SM 3	0.589±0.228	2.09±0.844	0.771±0.097
SM 4	0.580±0.238	2.19±0.851	0.733±0.115
SM 5	0.582±0.229	2.19±0.831	0.701±0.121
SM 6	0.599±0.231	1.98±0.829	0.790±0.110
SM 7	0.585±0.250	2.04±0.825	0.776±0.109
SM 8	0.593±0.207	2.01±0.839	0.788±0.107
SM 9	0.587±0.239	2.11±0.925	0.773±0.110
Mean±SD	0.59±0.003	2.06±0.032	0.77±0.010
DM			
DM 1	0.540±0.233	2.10±0.777	0.73±0.111
DM 2	0.558±0.206	2.18±0.843	0.76±0.106
DM 3	0.525±0.241	2.08±0.706	0.73±0.113
DM 4	0.565±0.242	2.07±0.632	0.71±0.118
DM 5	0.588±0.244	2.09±0.917	0.77±0.111
DM 6	0.571±0.230	2.01±0.743	0.75±0.127
DM 7	0.582±0.234	2.04±0.725	0.75±0.113
DM 8	0.567±0.229	2.12±0.804	0.74±0.109
DM 9	0.583±0.254	2.02±0.776	0.75±0.118
Mean±SD	0.56±0.007	2.08±0.018	0.75±0.007
Mann-Whitney test	0.003	0.605	0.050
Kuskall-Wallis test	0.004	0.799	0.068
One-way ANOVA	0.005	0.772	0.121

DM: Desmoplastic melanoma, SM: Spindle melanoma, SD: Standard deviation, ANOVA: Analysis of variance, bold values indicate significant differences

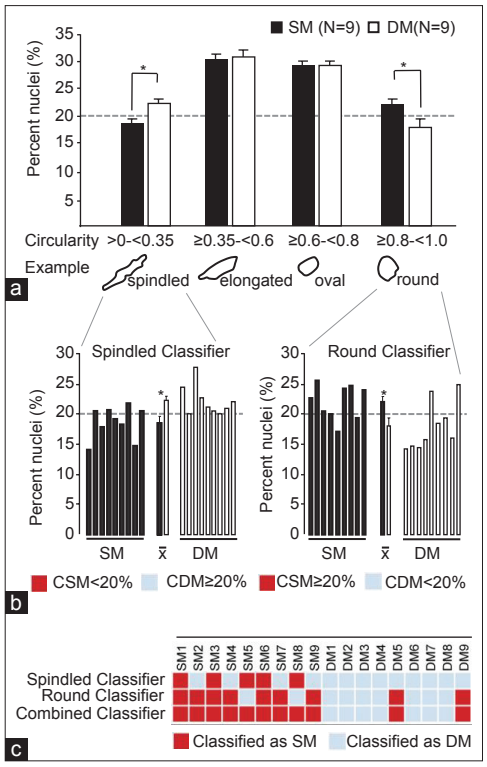

Figure 3: Nuclear circularity-based diagnostic classifier in spindle cell melanoma (SM) and desmoplastic melanoma (DM). (a) Cellular-shape classifier constructed as four distinct bins chosen based on the circularity value (shown along a representative nuclear outline). Plotted is the combined frequency distribution in each bin for all SM versus DM cases. Statistical comparison (*t*-test) showed no significant difference between SM versus DM when comparing elongated and oval; however, there were significant differences in the spindled and round category. (b) Threshold determination at the single case-level identified. Cut-off values in percent for the spindled (left) and round (right) classifier are provided as "classified as spindled melanoma (CSM)" or "classified as desmoplastic melanoma" (CDM) along with symbols. (c) Comparison of diagnostic classification based on the original morphological-(columns) and shape-based diagnosis (rows). The combined classifier followed the "believe the positive" rule and classified as SM was assigned when either test was positive

significant differences when opposite histotypes are compared [e.g. SM vs. DM; Figure 2b], whereas there are fewer differences when cases within one group (e.g. SM vs. SM). Such differences between histotypes (SM vs. DM), indicative of discriminatory power, were not present for aspect ratio and solidity [Figure 2b].

For a detailed examination of circularity values at a case-level, we compared histograms displaying the relative frequency of the circularity measurements [Figure 2c]. First, we noted that the distributions are non-Gaussian and demonstrate local peaks that correspond to the most common nuclear shape in the respective case. Notably, as compared to SM, DM showed a relatively higher amount of spindled nuclei. To create a diagnostic classifier based on these observations, circularity values were binned into four categories termed: Spindled, elongated, oval, and round (see methods). The relative percentage of nuclei in each bin is shown in Figure 3a and the elongated and oval bins showed no significant differences ($P = 0.77$; $P = 0.95$, respectively). However, when examining the spindled and round groups, paradoxically DM contained more spindled nuclei than SM (22.2% ±0.8% in DM vs. 18.6% ±0.9% in SM; $P = 0.011$) and SM contained more round nuclei than DM (22% ±1.0% in SM vs. 17.9% ±1.4% in DM; $P = 0.026$).

To determine diagnostic test performance, we decided to incorporate both the rounded and the spindled category into a combined classifier termed classified as SM (CSM). When examining the difference in the round and spindled category and accounting for the fact that most diagnostic pathologist apply 10%-steps when quantifying microscopic information, we set the cut-off to 20% [Figure 3b and c]. Specifically, the case was considered positive when containing less than 20% spindled nuclei or more than 20% round nuclei. In other words, if one or both of the criteria are met, the case is CSM. With these assignments of the shape-based classifier, comparison to the original morphological diagnosis was possible [Figure 3d]. Results of the overall

Table 3: Diagnostic test performance of the developed SM classifier

Variable	SM classifier (CSM)
	Number of cases=18
True positive	9
False positive	2
True negative	7
False negative	0
Sensitivity (95% CI)	100 (62.9-100)
Specificity (95% CI)	77.8 (40.2-96.1)
PPV (95% CI)	81.8 (47.8-96.8)
NPV (95% CI)	100 (56.1-100)
Accuracy	88.9
Pretest odds positive	1
Posttest odds positive	4.5
Youden index	0.77

CI: Confidence interval, PPV: Positive predictive value, NPV: Negative predictive value, CSM: Classified as spindle cell melanoma, SM: Spindle cell melanoma

test performance calculations are shown in Table 3. Briefly, performance measures are substantial and with an overall accuracy of 89% and a Youden index of 0.77, our data point out that nuclear circularity-based quantification can be applied as an adjunct diagnostic tool.

DISCUSSION

Here, we report that quantification of nuclear circularity in DM and SM demonstrated significant differences in the fraction of round and spindled nuclei in these melanoma subtypes. SM is characterized by a relatively higher fraction of round nuclei whereas DM is characterized by a relatively higher fraction of spindled nuclei. The proposed classifier demonstrates substantial test performance measures and is relatively straightforward. The required computational tools are freely available, user-friendly, and well-established, all of which argues for the implementation as a diagnostic aid, when necessary.

Examination of nuclear shapes is one of the key components in every histopathological examination. Specifically, variation in nuclear shape is a distinct feature of malignancy, and anisonucleosis a key feature of many neoplasias. Notably, nuclear grading is not established in the setting of SM/DM – neither is it in the setting of melanoma in general, probably in part due the broad spectrum of morphologies (i.e. melanoma as the "great imitator").[43] With respect to automated quantification of microscopic information, nuclear morphometry is clearly a useful diagnostic tool in several settings.[16-21,26,27] Automated quantification of microscopic information can uncover differences not necessarily captured visually;[44] and in reverse, qualitative morphological impressions are hard to compare or quantify. Here, we applied a nuclear circularity-based classifier to confirm a morphological impression of the variation in nuclear shapes between SM and DM. Despite the name, we found that DM contains more spindled shaped nuclei when compared to SM – and in reverse that SM contained more round nuclei than DM [Figure 3a]. Clearly some overlap of shapes between the groups did exist and suggested that studies on a larger number of cases, examination in mixed-or unknown cases may be interesting to further investigate the nuclear morphometry and its diagnostic value in this specific context.

From a biological perspective, it is noteworthy to mention that gene-sets that promote rounding of cells have recently been reported.[2] Clearly, such combinations of genetic, and morphological data provide insights into the underlying molecular machinery orchestrating cellular- and nuclear shapes; however, we are at this point not aware of a cellular SM/DM model or system to examine whether similar genetic programs are at play. Nonetheless, many of the genes that are part of this conserved shaping program (e.g. PTEN, MAPK, JAK) have clear roles in melanoma.[45]

Technically, the applied circularity classifier is simple and easy to use – yet, as with other morphometric software tools, some constraints apply and have to be taken into account. First, morphometry requires well-fixed samples, expert sectioning and reliable staining. However, in routine diagnostics this is not always achievable, and specimens may be cauterized, sections folded and staining heterogeneous. Second, given that the circularity classifier works on light-microscopic images- scanning and image acquisition as well as correction have to be performed and can introduce errors such as blurred regions. Third, the histological content itself can impose problems; for example, hypercellular regions with nuclear molding or inflammatory infiltrates. While we can account for some of these constraints (e.g., by the choice of region of interest), clearly not all of these variations can be accounted for and one can summarize these aspects that ultimately limit the quality of the downstream results as: "garbage in – garbage out."[46]

From an image analysis standpoint, our ImageJ-based algorithm,[41] combines well-established analytical functions and requires only a routine personal computer with Java and other widely available software packages (see methods). While we automated some of the steps in our analyses, there are numerous sophisticated algorithms[1-3,7,8,23,24,27,47,48] and examples of excellent software applications that are in part freely available. Some examples include TMARKER,[47] cellprofiler[49] or matlab.[50,51] The versatility of these programs is impressive; however, at the same time they require a kind of expertise that, at least currently, lays out of scope for most diagnostic, surgical pathologist. The chosen approach

is relatively easy to use; however, the applied plugins, and in particular the extraction of the nuclear outlines carries limitations. As illustrated in Figure 2a (top right), prominent nucleoli, irregular chromatic, anisochromasia and nuclear outline irregularities, cannot be precisely extracted by the simple threshold-based extraction. Clearly there are more sophisticated approaches for feature extraction; however, from a statistical perspective these 'limitations' actually increase the stringency of our study. Since our study was triggered by the observation that SM carries more round nuclei, the "weakness" of our threshold-based extraction actually introduced even more "nonround" elements in this melanoma subtype. Accepting these additional constraints in our analysis, demonstration of a significantly higher fraction of round particles in SM, actually represents, statistically speaking, the more pessimistic assumption.[42] Thus, our study may trigger verification, ideally performed by other laboratories or applying more sophisticated approached. However, the starting point for this study was a simple morphological impression (nuclear circularity variation) that we confirmed using easy-to-use and freely available tools. Having said that, we still want to point out that our nuclear circularity-based classifier should not replace careful and state-of-the-art evaluation by a trained pathologist – especially for diagnostic distinction of difficult cases. In these difficult settings we foresee that information from adjunct digital tools may become increasingly useful.

In summary, we present a nuclear circularity-based classifier of SM and DM that can be applied as an adjunct digital tool for diagnostic distinction in this setting.

ACKNOWLEDGMENTS

The authors would like to thank Birgit Rettenmaier and Dr. Ulrike Kostezka for expert technical assistance. Furthermore, we would like to thank Michael Held for help with slide-scanning. ARB is supported by Evangelisches Studienwerk e.V.; and the Else-Kröner Fresenius foundation supports JKL.

REFERENCES

1. Battich N, Stoeger T, Pelkmans L. Image-based transcriptomics in thousands of single human cells at single-molecule resolution. Nat Methods 2013;10:1127-33.
2. Yin Z, Sadok A, Sailem H, McCarthy A, Xia X, Li F, *et al.* A screen for morphological complexity identifies regulators of switch-like transitions between discrete cell shapes. Nat Cell Biol 2013;15:860-71.
3. Irshad H, Veillard A, Roux L, Racoceanu D. Methods for nuclei detection, segmentation, and classification in digital histopathology: A review-current status and future potential. IEEE Rev Biomed Eng 2014;7:97-114.
4. Rosai J. Why microscopy will remain a cornerstone of surgical pathology. Lab Invest 2007;87:403-8.
5. Thorstenson S, Molin J, Lundström C. Implementation of large-scale routine diagnostics using whole slide imaging in Sweden: Digital pathology experiences 2006-2013. J Pathol Inform 2014;5:14.
6. Murphy WM. Anatomical pathology in the 21st century: The great paradigm shift. Hum Pathol 2007;38:957-62.
7. Fuchs TJ, Buhmann JM. Computational pathology: Challenges and promises for tissue analysis. Comput Med Imaging Graph 2011;35:515-30.
8. Fuchs TJ, Wild PJ, Moch H, Buhmann JM. Computational pathology analysis of tissue microarrays predicts survival of renal clear cell carcinoma patients. Med Image Comput Comput Assist Interv 2008;11:1-8.
9. Schwartz J, Haffner S. ePathology: Defining the new paradigm of anatomic pathology. MLO Med Lab Obs 2013;45:30-1.
10. Daniel C, Macary F, Rojo MG, Klossa J, Laurinavicius A, Beckwith BA, *et al.* Recent advances in standards for Collaborative Digital Anatomic Pathology. Diagn Pathol 2011;6 Suppl 1:S17.
11. Brachtel E, Yagi Y. Digital imaging in pathology – current applications and challenges. J Biophotonics 2012;5:327-35.
12. Chen Y, Liang CP, Liu Y, Fischer AH, Parwani AV, Pantanowitz L. Review of advanced imaging techniques. J Pathol Inform 2012;3:22.
13. Skaland I, Øvestad I, Janssen EA, Klos J, Kjellevold KH, Helliesen T, *et al.* Comparing subjective and digital image analysis HER2/neu expression scores with conventional and modified FISH scores in breast cancer. J Clin Pathol 2008;61:68-71.
14. Masmoudi H, Hewitt SM, Petrick N, Myers KJ, Gavrielides MA. Automated quantitative assessment of HER-2/neu immunohistochemical expression in breast cancer. IEEE Trans Med Imaging 2009;28:916-25.
15. Tuominen VJ, Tolonen TT, Isola J. ImmunoMembrane: A publicly available web application for digital image analysis of HER2 immunohistochemistry. Histopathology 2012;60:758-67.
16. Acker SM, Nicholson JH, Rust PF, Maize JC. Morphometric discrimination of melanoma *in situ* of sun-damaged skin from chronically sun-damaged skin. J Am Acad Dermatol 1998;39:239-45.
17. Natarajan S, Mahajan S, Boaz K, George T. Prediction of lymph node metastases by preoperative nuclear morphometry in oral squamous cell carcinoma: A comparative image analysis study. Indian J Cancer 2010;47:406-11.
18. Ozcan A, Kurt B, Karslioglu Y, Cermik AH, Firat AB. Nuclear morphometry in the differential diagnosis of eosinophilic renal epithelial tumors. Anal Quant Cytol Histol 2012;34:145-8.
19. Talve LA, Collan YU, Ekfors TO. Nuclear morphometry, immunohistochemical staining with Ki-67 antibody and mitotic index in the assessment of proliferative activity and prognosis of primary malignant melanomas of the skin. J Cutan Pathol 1996;23:335-43.
20. Veltri RW, Christudass CS. Nuclear morphometry, epigenetic changes, and clinical relevance in prostate cancer. Adv Exp Med Biol 2014;773:77-99.
21. Veta M, Kornegoor R, Huisman A, Verschuur-Maes AH, Viergever MA, Pluim JP, *et al.* Prognostic value of automatically extracted nuclear morphometric features in whole slide images of male breast cancer. Mod Pathol 2012;25:1559-65.
22. Mijovic Z, Kostov M, Mihailovic D, Zivkovic N, Stojanovic M, Zdravkovic M. Correlation of nuclear morphometry of primary melanoma of the skin with clinicopathological parameters and expression of tumor suppressor proteins (p53 and p16(INK4a)) and bcl-2 oncoprotein. J BUON 2013;18:471-6.
23. Rangamani P, Xiong GY, Iyengar R. Multiscale modeling of cell shape from the actin cytoskeleton. Prog Mol Biol Transl Sci 2014;123:143-67.
24. Rangamani P, Lipshtat A, Azeloglu EU, Calizo RC, Hu M, Ghassemi S, *et al.* Decoding information in cell shape. Cell 2013;154:1356-69.
25. Neves SR, Tsokas P, Sarkar A, Grace EA, Rangamani P, Taubenfeld SM, *et al.* Cell shape and negative links in regulatory motifs together control spatial information flow in signaling networks. Cell 2008;133:666-80.
26. de Andrea CE, Petrilli AS, Jesus-Garcia R, Bleggi-Torres LF, Alves MT. Large and round tumor nuclei in osteosarcoma: Good clinical outcome. Int J Clin Exp Pathol 2011;4:169-74.
27. Song J, Shea CR. Benign versus malignant parakeratosis: A nuclear morphometry study. Mod Pathol 2010;23:799-803.
28. Weissinger SE, Keil P, Silvers DN, Klaus BM, Möller P, Horst BA, *et al.* A diagnostic algorithm to distinguish desmoplastic from spindle cell melanoma. Mod Pathol 2014;27:524-34.
29. Kossard S, Wilkinson B. Nucleolar organizer regions and image analysis nuclear morphometry of small cell (nevoid) melanoma. J Cutan Pathol 1995;22:132-6.

30. Karbowniczek M, Chosia M, Domagala W. Nuclear morphometry of MIB-1 positive and negative tumor cells in primary and metastatic malignant melanoma of the skin. Pol J Pathol 1999;50:235-41.
31. Williams RA, Baak JP, Meijer GA, Charlton IG. DNA ploidy and nuclear morphometry for the classification of dysplastic nevi. Anal Quant Cytol Histol 1999;21:437-44.
32. McCarthy SW, Crotty KA, Scolyer RA. Desmoplastic melanoma and desmoplastic neurotropic melanoma. In: LeBoit PE, editor. Pathology and Genetics of Skin Tumours. Lyon: IARC Press; 2006.
33. McCarthy SW, Scolyer RA, Palmer AA. Desmoplastic melanoma: A diagnostic trap for the unwary. Pathology 2004;36:445-51.
34. Coupelon S, Franck F, Jarrousse AS, Déchelotte P, Souteyrand P, D'Incan M. Desmoplastic malignant melanoma: A study of ten cases and status of BRAF mutation. Dermatology 2012;225:168-71.
35. Longacre TA, Egbert BM, Rouse RV. Desmoplastic and spindle-cell malignant melanoma. An immunohistochemical study. Am J Surg Pathol 1996;20:1489-500.
36. Lennerz JK, Kim SH, Oates EL, Huh WJ, Doherty JM, Tian X, *et al.* The transcription factor MIST1 is a novel human gastric chief cell marker whose expression is lost in metaplasia, dysplasia, and carcinoma. Am J Pathol 2010;177:1514-33.
37. Khan AM, Rajpoot N, Treanor D, Magee D. A nonlinear mapping approach to stain normalization in digital histopathology images using image-specific color deconvolution. IEEE Trans Biomed Eng 2014;61:1729-38.
38. Meyer AS, Dallenbach FE, Lienert G, Möller P, Lennerz JK. Application of digital pathology tools. An unusual case of non-Hodgkin lymphoma. Pathologe 2012;33 Suppl 2:200-4.
39. Shapiro LG, Stockman GC. Computer Vision. Upper Saddle River, NJ: Prentice Hall; 2001. p. xx, 580.
40. Lennerz JK, Rühle V, Ceppa EP, Neuhuber WL, Bunnett NW, Grady EF, *et al.* Calcitonin receptor-like receptor (CLR), receptor activity-modifying protein 1 (RAMP1), and calcitonin gene-related peptide (CGRP) immunoreactivity in the rat trigeminovascular system: Differences between peripheral and central CGRP receptor distribution. J Comp Neurol 2008;507:1277-99.
41. Schneider CA, Rasband WS, Eliceiri KW. NIH Image to ImageJ: 25 years of image analysis. Nat Methods 2012;9:671-5.
42. Rabinovich SG. Measurement Errors and Uncertainties: Theory and Practice. 2nd ed. New York, NY: AIP Press; 2000.
43. Pernick NL, DaSilva M, Gangi MD, Crissman J, Adsay V. Histiocytic markers in melanoma. Mod Pathol 1999;12:1072-7.
44. Snijder B, Pelkmans L. Origins of regulated cell-to-cell variability. Nat Rev Mol Cell Biol 2011;12:119-25.
45. Uzdensky AB, Demyanenko SV, Bibov MY. Signal transduction in human cutaneous melanoma and target drugs. Curr Cancer Drug Targets 2013;13:843-66.
46. O'Hurley G, Sjöstedt E, Rahman A, Li B, Kampf C, Pontén F, *et al.* Garbage in, garbage out: A critical evaluation of strategies used for validation of immunohistochemical biomarkers. Mol Oncol 2014;8:783-98.
47. Schüffler PJ, Fuchs TJ, Ong CS, Wild PJ, Rupp NJ, Buhmann JM. TMARKER: A free software toolkit for histopathological cell counting and staining estimation. J Pathol Inform 2013;4:S2.
48. Cruz-Roa AA, Arevalo Ovalle JE, Madabhushi A, González Osorio FA. A deep learning architecture for image representation, visual interpretability and automated basal-cell carcinoma cancer detection. Med Image Comput Comput Assist Interv 2013;16:403-10.
49. Carpenter AE, Jones TR, Lamprecht MR, Clarke C, Kang IH, Friman O, *et al.* CellProfiler: Image analysis software for identifying and quantifying cell phenotypes. Genome Biol 2006;7:R100.
50. Markiewicz T. Using MATLAB software with Tomcat server and Java platform for remote image analysis in pathology. Diagn Pathol 2011;6 Suppl 1:S18.
51. White AM, Daly DS, Willse AR, Protic M, Chandler DP. Automated Microarray Image Analysis Toolbox for MATLAB. Bioinformatics 2005;21:3578-9.